Interaction between Mitochondrial CYP27B1 and Adrenodoxin: Role of Arginine 458 of Mouse CYP27B1†

Naoko Urushino,‡ Keiko Yamamoto,§ Norio Kagawa,|| Shinichi Ikushiro,⊥ Masaki Kamakura,⊥ Sachiko Yamada,§ Shigeaki Kato,# Kuniyo Inouye,‡ and Toshiyuki Sakaki*,⊥

Division of Food Science and Biotechnology, Graduate School of Agriculture, Kyoto University, Sakyo-ku, Kyoto 606-8502, Japan, Institute of Biomaterials and Bioengineering, Tokyo Medical and Dental University, 2-3-10 Kanda-Surugadai, Chiyoda-ku, Tokyo 101-0062, Japan, Department of Biochemistry, Vanderbilt University School of Medicine, Nashville, Tennessee 37232-0146, Biotechnology Research Center, Faculty of Engineering, Toyama Prefectural University, 5180 Kurokawa, Imizu, Toyama 939-0398, Japan, and Institute of Molecular and Cellular Biosciences, Tokyo University, 1-1-1 Yayoi, Bunkyo, Tokyo 113-0032, Japan

Received January 12, 2006; Revised Manuscript Received February 23, 2006

ABSTRACT: A molecular modeling study of CYP27B1 suggests that Arg458 of mouse CYP27B1 is involved in interaction with adrenodoxin (ADX). Thus, we generated CYP27B1 mutants R458K and R458Q and revealed their enzymatic properties. Substrate-induced difference spectra and K_m values for 1α-hydroxylation of 25(OH)D_3 indicate that the replacement of Arg458 with Lys or Gln does not affect substrate binding. However, these mutants showed remarkable decreases of both k_{cat} values and the ratio of product formation to NADPH oxidation (coupling efficiency). A high K_m value of R458Q for ADX concentration and a decrease of rate constant of the first electron transfer seem reasonable considering that the conversion from Arg to noncharged Gln abolishes salt-bridge formation with the acidic residue of ADX. On the other hand, R458K showed atypical kinetics for ADX concentration with Hill's constant of 2.0 and high catalytic activity at high ADX concentration by increase of coupling efficiency. These results suggest that conformational change of R458K by binding the two ADX molecules is essential for 1α-hydroxylation of 25(OH)D_3. On the other hand, binding one ADX molecule is sufficient for the conformational change of the wild-type CYP27B1, judging from its Michaelis−Menten-type kinetics for ADX concentration with high coupling efficiency. These results suggest that ADX functions as an effector for the oxygen transfer reaction in addition to being an electron donor for CYP27B1.

A hormonally active form of vitamin D_3, 1α,25$(OH)_2D_3$,[1] plays essential roles in calcium homeostasis, immunology, and cell differentiation (*1*−*5*). 1α,25$(OH)_2D_3$ is produced by two-step hydroxylations at the 25-position in the liver by several types of cytochrome P450s including mitochondrial CYP27A1 (*6*) and microsomal CYP2R1 (*7*) and then at the 1α-position in the kidney by mitochondrial CYP27B1 (*8*).

On the inner membrane of the mitochondria, all mitochondrial P450s interact with a common electron donor, ADX, which is an acidic [2Fe-2S] ferredoxin-type protein. ADX functions as a single electron carrier between a FAD-containing NADPH-dependent adrenodoxin reductase (ADR) and different heme-bearing cytochrome P450s and participates in these cytochrome P450-catalyzed hydroxylation reactions to produce steroid hormones, vitamin D metabolites, and bile acids. Several electron transfer mechanisms in the mitochondrial P450 system have been suggested so far (*9*−*14*). According to the shuttle model, ADX serves as a mobile carrier between ADR and cytochrome P450 (*9*, *10*). Another shuttle model starts from an ADX dimer that transports either one or two electrons (*11*, *14*). Other models propose a ternary (1:1:1) and a quarternary (1:2:1) complex consisting of ADR, ADX, and P450 (*12*, *13*). According to the latter model, electron transfer can take place on the 1:2:1 complex as well as the shuttle model with the ADX dimer. It is, however, possible that different mechanisms are active in different mitochondrial P450 species. For the interactions between ADX and mitochondrial CYP11A1 and CYP27A1, it has been reported that several Lys and Arg residues play essential roles in electrostatic interaction with the acidic amino acid residues of ADX (*15*−*17*).

Recently, we successfully overexpressed recombinant mouse CYP27B1 and its mutants in *Escherichia coli* by a coexpression system with GroEL/ES (*18*). Using a three-dimensional CYP27B1 model, we studied the docking of 25-hydroxyvitamin D_3 in a substrate-binding pocket of CYP27B1. In a mutation study of mouse CYP27B1 including spectroscopic and enzymatic analyses, we concluded that, in a 1α-

† This work was supported in part by a Grant-in-Aid for Scientific Research from the Ministry of Education, Science, and Culture of Japan and by the Sankyo Foundation of Life Sciences.

* To whom correspondence should be addressed. Tel: +81-766-56-7500. Fax: +81-766-56-2498. E-mail: tsakaki@pu-toyama.ac.jp.
‡ Kyoto University.
§ Tokyo Medical and Dental University.
|| Vanderbilt University School of Medicine.
⊥ Toyama Prefectural University.
Tokyo University.

[1] Abbreviations: 25(OH)D_3, 25-hydroxyvitamin D_3; 1α,25$(OH)_2D_3$, 1α,25-dihydroxyvitamin D_3; CYP, cytochrome P450; ADX, adrenodoxin; ADR, NADPH−adrenodoxin reductase.

10.1021/bi060072o CCC: $33.50
Published on Web 03/18/2006

hydroxylation process, the Ser408 of mouse CYP27B1 corresponding to Thr409 of human CYP27B1 forms a hydrogen bond with the 25-hydroxyl group of 25-hydroxyvitamin D_3 (*19*). In this study, we demonstrate the amino acid residue responsible for interaction with ADX using a three-dimensional structure docking model of CYP27B1 and adrenodoxin.

EXPERIMENTAL PROCEDURES

Materials. DNA-modifying enzymes, restriction enzymes, and the DNA sequencing kit were purchased from Takara Shuzo Co., Ltd. (Kyoto, Japan). Primer DNAs for mutation were purchased from GENSET KK (Kyoto, Japan). *E. coli* DH5α (Takara Shuzo Co.) was used as a host strain. The pKSNdl was constructed from pkk223-3 as described previously (*20*). The GroEL/ES expression plasmid, pGro12, was kindly given by HSP Research Laboratory (Kyoto, Japan). CHAPS was purchased from Dojindo (Kumamoto, Japan). NADPH was purchased from Oriental Yeast Co. (Tokyo, Japan). Bovine ADX containing residues 1−114 of the mature form was kindly given by Dr. Y. Nonaka of Koshien University. 25(OH)D_3 was purchased from Wako Pure Chemical Industries, Ltd. (Osaka, Japan). Other chemicals used were of the highest quality commercially available.

Sequence Alignment and Molecular Modeling. Molecular modeling and graphical manipulations were performed by using SYBYL7.0 (Tripos Associates, St. Louis, MO) as described previously (*19*, *21*). Mouse CYP27B1 was aligned with human CYP27B1 by using ClustalW interfaced with Clustal X (version 1.81) for Windows. We constructed mouse CYP27B1 by the replacement method using human CYP27B1 as a template. Construction was carried out by using a mutation command, Mutate Monomers, of Biopolymer in SYBYL7.0. Since the residue corresponding to P353 of human CYP27B1 was deleted in mouse CYP27B1, R352 and G353 (corresponding to G354 of human CYP27B1) were directly joined. Energy minimization of the constructed structure was performed on the Tripos force field. The structure of mouse CYP27B1 was evaluated by using the PROCHECK program. The atomic coordinates of the crystal structure of bovine ADX were retrieved from the RCSB Protein Data Bank (PDB ID 1E6E). Electrostatic potential surface was calculated by Connolly surface command and then electrostatic potential command.

Construction of Expression Plasmids. The expression plasmid for mouse CYP27B1 with a His tag at the C-terminus, pKCHis-m1α, was constructed as described (*22*). The expression plasmids for CYP27B1 mutants (R457A, R458A, R458K, and R458Q) were generated by the QuickChange site-directed mutagenesis kit from Strategene (Amsterdam, The Netherlands) according to the instruction manual. The oligonucleotide primers for mutagenesis are shown in Table 1. Corrected generation of desired mutations was confirmed by DNA sequencing.

Cultivation of the Recombinant E. coli Cells. The *E. coli* DH5α harboring pGro12 was transformed with the expression plasmid for wild-type CYP27B1 (pKCHis-m1α) or its mutants. Recombinant *E. coli* cells were grown in TB media (pH 7.0) containing 50 μg/mL ampicillin and 25 μg/mL kanamycin at 26 °C under good aeration for 24 h. The induction of transcription of CYP27B1 cDNA and GroEL/ES gene was initiated by addition of IPTG and arabinose at a final concentration of 1 mM and 4 mg/mL, respectively. δ-Aminolevulinic acid was also added at a final concentration of 1 mM. The *E. coli* JM109/pKAR cells were used to produce bovine ADR (*23*). The recombinant cells were grown in TB-broth medium containing 50 μg/mL ampicillin at 26 °C under good aeration, and the induction of transcription of ADR cDNA was initiated by addition of IPTG at a final concentration of 1 mM.

Table 1: Oligonucleotides Used To Generate CYP27B1 Mutants

mutation	oligonucleotides
R457A	5′-GGAGCTGCATCGGGGCACGCTTGGCAGAGC-3′ 5′-GCTCTGCCAAGCGTGCCCCGATGCAGCTCC-3′
R458A	5′-CGGGAGAGCCTTGGCAG-3′ 5′-CTGCCAAGGCTCTCCCG-3′
R458K	5′-GCTGCATCGGGAGAAAGTTGGCAGAGCTTG-3′ 5′-CAAGCTCTGCCAACTTTCTCCCGATGCAGC-3′
R458Q	5′-GCTGCATCGGGAGACAATTGGCAGAGCTTG-3′ 5′-CAAGCTCTGCCAATTGTCTCCCGATGCAGC-3′

Solubilization of Wild-Type CYP27B1 and Mutants by CHAPS. The recombinant *E. coli* cells were suspended in 100 mM Tris-HCl buffer (pH 7.4) containing 1% CHAPS, 1 mM EDTA, 0.1 mM PMSF, and 20% glycerol and disrupted by sonication for 15 min at 4 °C. Cell debris was removed at 1200*g* for 10 min. Then the supernatant was ultracentrifugated at 100000*g* for 1 h at 4 °C. The resultant supernatant was used for spectral and enzymatic analyses.

Purification of Wild-Type CYP27B1 and Mutants. The fractions containing the solubilized CYP27B1 were applied to a Ni−Sepharose high-performance device (Amersham Bioscience) equilibrated with 100 mM Tris-HCl buffer (pH7.4) containing 0.5% CHAPS, 1 mM EDTA, and 20% glycerol (buffer A) at a flow rate of 1 mL/min. After adsorption of CYP27B1, the column was washed with about 10 column volumes of buffer A and the same volumes of buffer A containing 20 mM imidazole, and then CYP27B1 was eluted with a linear gradient of 20−500 mM imidazole in buffer A (10 column volumes). Finally, the eluted CYP27B1 was applied to a PD-10 column to remove imidazole.

Purification of NADPH−Adrenodoxin Reductase. The recombinant *E. coli* cells expressing ADR were suspended in 10 mM potassium phosphate buffer (pH 7.4) and disrupted by sonication for 15 min at 4 °C. After centrifugation at 1200*g* for 10 min, the supernatant was ultracentrifugated at 100000*g* for 1 h at 4 °C. The resultant supernatant containing ADR was applied to a DEAE-Sepharose high-performance device (Amersham Bioscience) equilibrated with 10 mM KP_i buffer (pH 7.4) at a flow rate of 2 mL/min. After adsorption of ADR, the column was washed with about 5 column volumes of 10 mM KP_i buffer (pH 7.4), and then ADR was eluted with a linear gradient of 0−1.0 M NaCl in 10 mM KP_i buffer (pH 7.4). The fractions containing ADR were collected and dialyzed with 10 mM KP_i buffer (pH 7.2) containing 0.1 M NaCl and then applied to a 2′,5′-ADP−Sepharose 4B column (Amersham Bioscience). After adsorption of ADR, the column was washed with about 10 column volumes of 10 mM KP_i buffer containing 0.1 M NaCl, and then ADR was eluted with a linear gradient of 0.1−1.0 M NaCl in 10 mM KP_i buffer (pH 7.4). Finally, the eluted ADR

was concentrated by centrifugation at 5000*g* using Amicon Ultra (Millipore). The expression levels of ADR were 30−50 nmol/L of culture. The purified sample of ADR showed almost a single band at 54 kDa on SDS−polyacrylamide gel (data not shown).

Measurement of CO Difference Spectra. CO difference spectra of reduced P450 were measured by a Hitachi U-3310 spectrophotometer with a head-on photomultiplier (Tokyo, Japan). The concentration of the CYP27B1 was determined from the CO difference spectrum of reduced P450 using a difference of extinction coefficient at 448 and 490 nm of 91 mM^{-1} cm^{-1} by Omura and Sato (*24*).

Measurement of Substrate-Induced Difference Spectra. Substrate-induced difference spectra of the wild-type CYP27B1 and mutants were measured in the presence of 1.0 μM 25(OH)D_3 by a Hitachi U-3310 spectrophotometer (Tokyo, Japan).

Measurement of Hydroxylation Activity toward 25(OH)-D_3. The 1α-hydroxylation activity toward 25(OH)D_3 was measured in the reconstituted system containing the purified sample of wild type (0.01 μM) or R458K (0.05 μM) or R458Q (0.05 μM) with 2.0 μM ADX, 0.2 μM ADR, and 0.05−1.0 μM 25(OH)D_3 for determination of kinetic parameters for 25(OH)D_3 concentration. On the other hand, the activity was measured in the reconstituted system containing the purified sample of wild type (0.001 μM) or R458K (0.001 μM) or R458Q (0.01 μM) with 0.5−50 μM ADX, 0.05−5 μM ADR, and 1.0 μM 25(OH)D_3 used for determination of kinetic parameters for ADX and ADR concentrations in 100 mM Tris-HCl (pH 7.4), 1 mM EDTA, 0.2% glycerol, and 0.1% CHAPS in a final volume of 0.5 mL. The ratio of ADX to ADR was fixed to 10. The optimal concentration of CHAPS was determined on the basis of our previous study (*18*). After incubation at 37 °C for 3 min, the reaction was initiated by adding NADPH at a final concentration of 1 mM and terminated by adding 2 mL of chloroform/methanol (3:1 v/v). After extraction, the organic phase was recovered and dried. The resulting residue was solubilized with acetonitrile and applied to HPLC under the following conditions: column, YMC-Pack ODS-AM (4.6 × 300 mm) (YMC Co., Tokyo, Japan); column temperature, 40 °C; mobile phase, linear gradient of 70−100% acetonitrile aqueous solution per 15 min; flow rate, 1.0 mL/min; UV detection, 265 nm. The kinetic parameters, K_m and k_{cat}, were calculated by the nonlinear regression analysis using the Kaleida-Graph (Synergy software).

Measurement of the NADPH-Dependent Reduction Rate of CYP27B1 and Its Mutants. The mixture containing the purified sample of wild type or each of its mutants at a final concentration of 0.2 μM, 5 μM 25(OH)D_3, 1 μM ADX, 0.2 μM ADR, 2% glycerol, 0.1% CHAPS in 100 mM Tris-HCl (pH 7.4), and 1 mM EDTA was poured into two cuvettes. After baseline correction and CO bubbling into the sample cuvette, NADPH was added to both cuvettes at the same time to a final concentration of 0.2 mM, and after mixing immediately, the change in absorbance difference between 448 and 490 nm was measured for 30 min at 25 °C. A computer program was employed to fit the kinetic data to the equation:

$$\Delta A_{448-490}(t) = \Delta A_{448-490}(\infty)[1 - \exp(-kt)] \quad (1)$$

where $\Delta A(t)$ is the observed change in absorbance at time t. The rate constant k (s^{-1}) indicates the efficiency of the first electron transfer from ADX.

Measurement of Consumption of NADPH during 1α-Hydroxylation of 25(OH)D_3. The reaction buffer consisting of 100 mM Tris-HCl (pH 7.4) and 1 mM EDTA was poured into two cells, the baseline was corrected, and then the purified sample of CYP27B1 or its mutant, ADX, ADR, and 25(OH)D_3 were added at the final concentration of 0.2, 1.0, 0.2, and 5.0 μM, respectively. The reaction mixture also contained CHAPS and glycerol at a final concentration of 0.1% and 2%, respectively. To initiate the reaction, NADPH was added to both cells at a final concentration of 0.2 mM, and the difference spectrum from 240 to 700 nm was measured at 25 °C for 15 min at intervals of 2 min. The absorbance difference between 340 and 400 nm was plotted against time and fitted to a linear equation to estimate the consumption rate of NADPH. At 15 min after the addition of NADPH, chloroform was added to terminate the reaction and extract the metabolites of 25(OH)D_3. After extraction, the organic phase was recovered and dried. The resulting residue was solubilized with acetonitrile and applied to HPLC under the following conditions: column, YMC-Pack ODS-AM (4.6 × 300 mm) (YMC Co., Tokyo, Japan); column temperature, 40 °C; mobile phase, linear gradient of 70−100% acetonitrile aqueous solution per 15 min; flow rate, 1.0 mL/min; UV detection, 265 nm.

Other Methods. The concentrations of vitamin D_3 derivatives were estimated by their molar extinction coefficient of 1.80×10^4 M^{-1} cm^{-1} at 264 nm (*25*). Total protein concentrations were determined by the Bradford method using bovine serum albumin as a standard. The concentrations of ADX and ADR were determined by molar extinction coefficients of 9.8 mM^{-1} cm^{-1} at 414 nm and 10.9 mM^{-1} cm^{-1} at 450 nm, respectively (*26*). The amino acid sequences of CYP11A1, CYP11B1, CYP11B2, CYP24A1, CYP27A1, and CYP27B1 were aligned by using Clustal W interfaced with Clustal X (version 1.81) for Windows.

RESULTS

Three-Dimensional Structure of Mouse CYP27B1. We compared both human and mouse CYP27B1 within residues between D39 and R508 where the 3D structure of human CYP27B1 is available (*20*, *21*). We found that sequence identity between D36 and R508 is 84% in both CYPs and only a single residue corresponding to P353 of human CYP27B1 is deleted from mouse CYP27B1, indicating that both CYPs would adopt quite similar architecture. Therefore, we constructed mouse CYP27B1 by the replacement method using human CYP27B1 as a template (Figure 1). We evaluated the model structure by using the PROCHEK program. A Ramachandran plot of mouse CYP27B1 showed 97.2% of the residues in either the most favored or allowed regions. The proximal side of mouse CYP27B1 as well as human CYP27B1 has a cavity which looks like adopting to the negatively charged surface of ADX. As shown in Figure 1, the surface of the cavity of mouse CYP27B1 bears four positively charged residues, K370, K374, R457, and R458, implying that these residues interact with the negatively charged residues of ADX.

Expression and Purification of Wild-Type CYP27B1 and Mutants. A molecular modeling study of CYP27B1 suggests

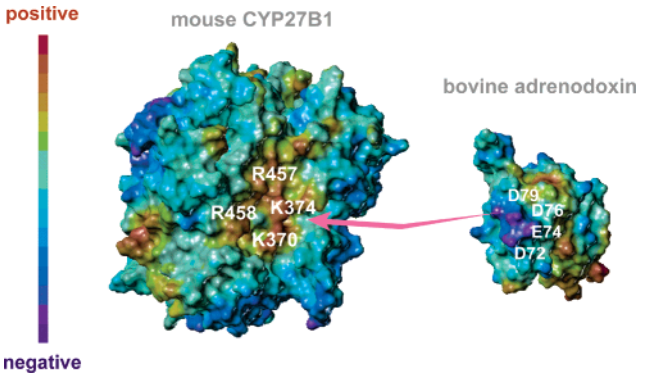

FIGURE 1: Electrostatic potential surface of mouse CYP27B1 and bovine ADX. The four positively charged residues located on the proximal surface of mouse CYP27B1, K370 and K374 in the K-helix and R457 and R458 in the L-helix, appear to be involved in the electrostatic interaction with four negatively charged amino acid residues of ADX, Asp72, Glu74, Asp76, and Asp79.

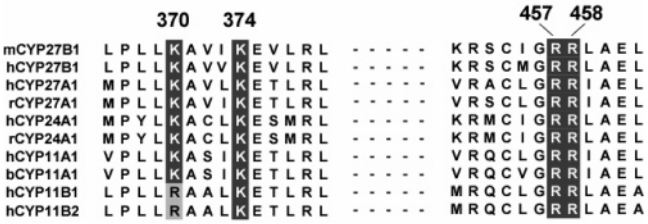

FIGURE 2: Comparison of the amino acid sequences of mouse CYP27B1 with other mitochondrial cytochromes P450. The four positively charged residues of mouse CYP27B1, K370, K374, R457, and R458, are highly conserved among mitochondrial CYPs. The residues that are identical and homologous in all of the CYPs are in dark and light shading, respectively.

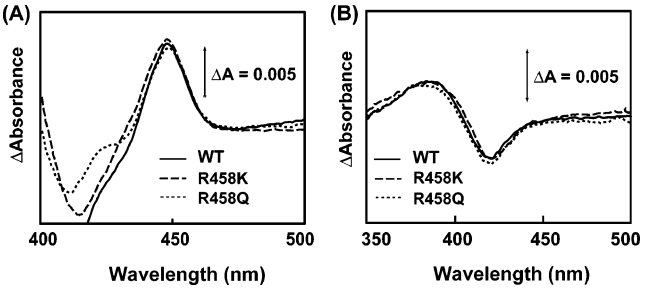

FIGURE 3: CO difference spectra (A) and substrate-induced difference spectra with 1.0 μM 25(OH)D$_3$ (B) of wild-type CYP27B1 (−) and mutants R458K (− −) and R458Q(- - -) at a P450 concentration of 0.1 μM. The difference spectra were measured in 100 mM Tris-HCl buffer (pH7.4) containing 0.1% CHAPS as described in Experimental Procedures.

that Arg457 and Arg458 of mouse CYP27B1 corresponding to Arg458 and Arg459 of human CYP27B1, respectively, are involved in interaction with ADX (Figure 1). These amino acid residues were conserved among all mitochondrial P450s (Figure 2). To reveal each function of these amino acid residues, we generated mutants of CYP27B1 at positions 457 and 458 of mouse CYP27B1. As shown in Figure 3A, the mutants R458K and R458Q showed CO difference spectra similar to that of the wild type. The expression level of wild-type CYP27B1 determined by the CO difference spectra was 200−300 nmol/L of culture, as described previously (*18*). The expression levels of R458A, R458K, and R458Q were nearly the same as that of the wild type. On the other hand, the expression level of the mutant R457A was too low to be determined by the CO difference spectra.

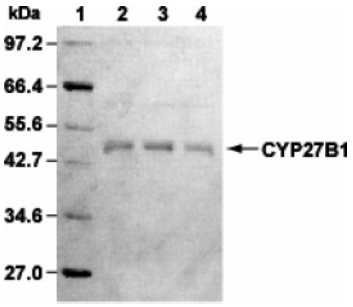

FIGURE 4: SDS−PAGE analysis of purified samples of wild-type CYP27B1 (lane 2) and mutants R458K (lane 3) and R458Q (lane 4). Lane 1 shows relative molecular mass markers (rabbit phosphorylase *b*, M_r 97200; bovine serum albumin, M_r 66400; bovine glutamic dehydrogenase, M_r 55600; *E. coli* maltose-binding protein, M_r 42700; *E. coli* thioredoxin reductase, M_r 34600; *E. coli* triosephosphate isomerase, M_r 27000).

Table 2: Kinetic Parameters for 25(OH)D$_3$ 1α-Hydroxylation Activity

	K_m (μM)	k_{cat} (min^{-1})
WT	0.38 ± 0.07	3.8 ± 2.5
R458K	0.33 ± 0.05	0.012 ± 0.005
R458Q	0.34 ± 0.13	0.021 ± 0.004

These results are consistent with the results observed in CYP11A1 reported by Usanov et al. (*17*). Thus, Arg457 appears to be involved in protein folding. The purified samples of wild type, R458K, and R458Q showed almost a single band at 51 kDa on SDS−polyacrylamide gel (Figure 4).

Analysis of Substrate Binding of Wild-Type CYP27B1 and Arg458 Mutants with 25(OH)D$_3$. As shown in Figure 3B, the mutants R458K and R458Q showed type I spectra quite similar to that of the wild type, indicating the change of spin state of heme iron of CYP27B1 from low spin to high spin by binding of 25(OH)D$_3$. These results suggest that the substrate, 25(OH)D$_3$, can remove the H_2O molecule as the sixth axial ligand of heme iron of wild-type CYP27B1 and the mutants R458K and R458Q.

Analysis of 1α-Hydroxylation Activity of Wild-Type CYP27B1 and Mutants toward 25(OH)D$_3$. The 1α-hydroxylation activity toward 25(OH)D$_3$ was examined using purified CYP27B1 as described in Experimental Procedures. As shown in Table 2, the kinetic parameters, K_m and k_{cat}, of the wild-type CYP27B1 were estimated to be 0.38 μM and 3.8 min^{-1}, respectively. The K_m values of R458K and R458Q were similar to that of the wild-type CYP27B1, suggesting that the affinity for 25(OH)D$_3$ is not affected by the substitution of Arg458 of mouse CYP27B1 toward Lys and Gln. In contrast, the k_{cat} values of these mutants are significantly lower than that of the wild type. It is noted that the k_{cat} value of R458K is lower than that of R458Q. On the other hand, R458A showed no detectable activity, whereas R458A showed a substrate-induced difference spectrum similar to that of the wild-type CYP27B1 (data not shown).

NADPH-Dependent Reduction of Heme Iron of Wild-Type CYP27B1 and Mutants. The NADPH-dependent CO difference spectra of wild type, R458K, and R458Q showed a maximum at 448 nm. In contrast, R458Q showed a maximum at 420 nm in addition to 448 nm, suggesting the instability of the CO-ferrous or ferrous form of R458Q. The plots of $\Delta A_{448-490}$ in Figure 5 were optimally fitted to eq 1

Table 3: NADPH-Dependent Reduction Rate of Heme Iron, Coupling Efficiency between Product Formation and NADPH Oxidation, and Kinetic Parameters for ADX Concentration on 25(OH)D_3 1α-Hydroxylation Activity

		coupling efficiency between product formation and NADPH oxidation			kinetic parameters for ADX concn	
	NADPH-dependent reduction rate k (s^{-1})	υ [mol min^{-1} (mol of P450)$^{-1}$]	NADPH oxidation rate [mol min^{-1} (mol of P450)$^{-1}$]	coupling (%)	$K_{m,ADX}$[a] (μM)	k_{cat} (min^{-1})
WT	0.0145	1.3 ± 0.2	6.5 ± 1.1	21 ± 7	9.5 ± 0.7	10.4 ± 1.6
R458K	0.0055	0.022 ± 0.015	0.58 ± 0.28	3.6 ± 0.9	34.0 ± 12.9	3.4 ± 0.7
R458Q	0.0026	0.029 ± 0.010	5.2 ± 2.3	0.58 ± 0.07	347 ± 19	0.80 ± 0.01

[a] Wild type and R458Q showed Michaelis−Menten-type kinetics with the equation $\upsilon = V_{max}[ADX]/(K_m + [ADX])$, while the kinetic data of R458K were fitted to Hill's equation $\upsilon = V_{max}[ADX]^2/(K_m^2 + [ADX]^2)$.

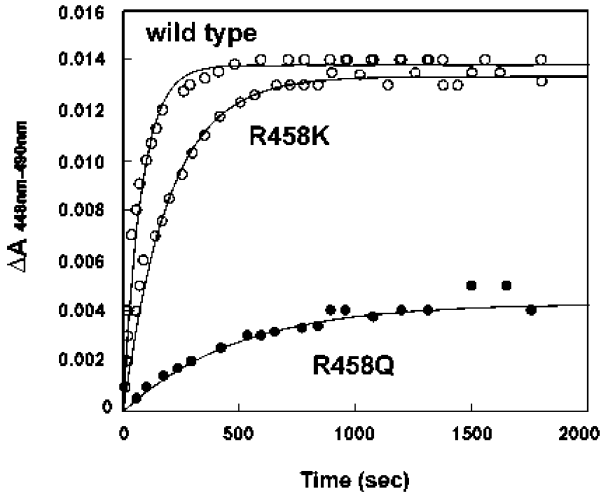

FIGURE 5: NADPH-dependent reduction of heme iron of wild-type CYP27B1 (open circles) and mutants R458K (shaded circles) and R458Q (filled circles) was measured in the mixture containing the purified sample of mouse CYP27B1 or each of its mutants at a final concentration of 0.2 μM with 5 μM 25(OH)D_3, 1 μM ADX, and 0.2 μM ADR. After addition of NADPH at a final concentration of 0.2 mM, $\Delta A_{448-490}$ was measured as described in Experimental Procedures. The plots of $\Delta A_{448-490}$ were optimally fitted to the equation $\Delta A_{448-490}(t) = \Delta A_{448-490}(\infty)[1 - \exp(-kt)]$.

as described in Experimental Procedures. The rate constant k in the wild type was estimated to be 0.0145 s^{-1} while those of R458K and R458Q were estimated to be 0.0055 and 0.0026 s^{-1}, respectively (Table 3). These results suggest that the substitution of Arg458 toward Lys decreases the efficiency of the first electron transfer. However, the dramatically decreased 1α-hydroxylation activity of R458K mentioned above cannot be fully explained by the slow reduction rate of heme iron. The apparent rate constant k of R458Q was estimated to be 18% of the wild type. Note that the magnitude of the maximum at 448 nm was about 30% of the wild type. Judging from the time course of R458Q in Figure 5, 70% of R458Q appears to be converted to P420.

Analysis of Coupling Efficiency between Product Formation and NADPH Oxidation. Table 3 shows the ratio of the product formation to NADPH oxidation measured in the reconstitution system containing 1 μM ADX, 0.2 μM ADR, 0.2 μM purified CYP27B1, 5 μM 25(OH)D_3, and 0.2 mM NADPH. The coupling efficiency of the wild type was 21%. In contrast, the NADPH oxidation rate of R458K was about 11-fold less than the wild type, and the coupling efficiency of R458K was about 6-fold less than the wild type. On the other hand, the NADPH oxidation rate of R458Q was similar to the wild type, although its 1α-hydroxylation activity toward 25(OH)D_3 was about 45-fold less than the wild type. Thus, the coupling efficiency of R458Q was dramatically decreased. It is assumed that R458Q produced a superoxide anion, hydrogen peroxide, or water instead of the formation of 1α,25(OH)$_2D_3$ (Figure 7). In addition, it might be possible to assume that R458Q enhances electron leakage from NADPH to O_2 via ADR and ADX (*28*, *29*).

1α-Hydroxylation Activity of Wild-Type CYP27B1 and Mutants in the Presence of Various Amounts of ADX and ADR. When the ADR concentration is insufficient to maintain ADX in the fully reduced state, the catalytic activity of P450 is dramatically decreased upon the inhibitory effect of oxidized ADX (*27*). However, an excess amount of ADR also inhibits the activity. On the basis of our results that a

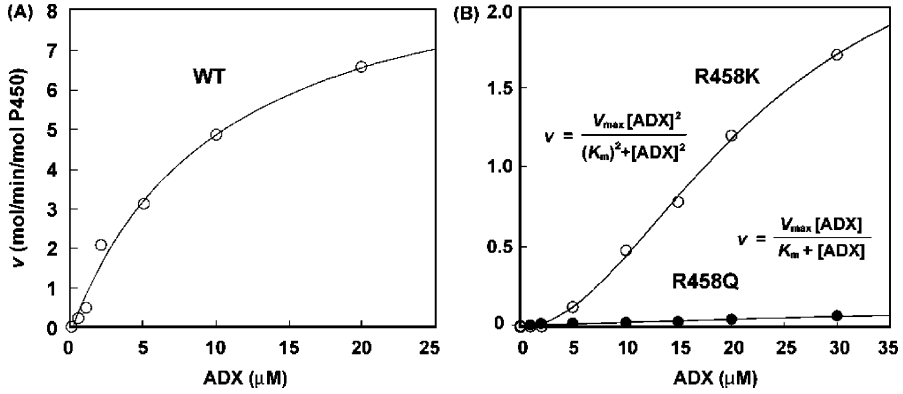

FIGURE 6: ADX dependency of catalytic activity of wild-type CYP27B1 (A) and mutants R458K and R458Q (B). 1α-Hydroxylation activity toward 25(OH)D_3 of wild-type CYP27B1 and the mutants was measured in the reconstituted system containing various amounts of ADX and ADR at a ratio of 10:1 as described in Experimental Procedures. The kinetic data of R458K were fitted to Hill's equation $\upsilon = V_{max}[ADX]^n/(K_m^n + [ADX]^n)$, and Hill's constant n was estimated to be 2.0, while the kinetic parameters of the wild type and R458Q were calculated with the Michaelis−Menten equation $\upsilon = V_{max}[ADX]/(K_m + [ADX])$.

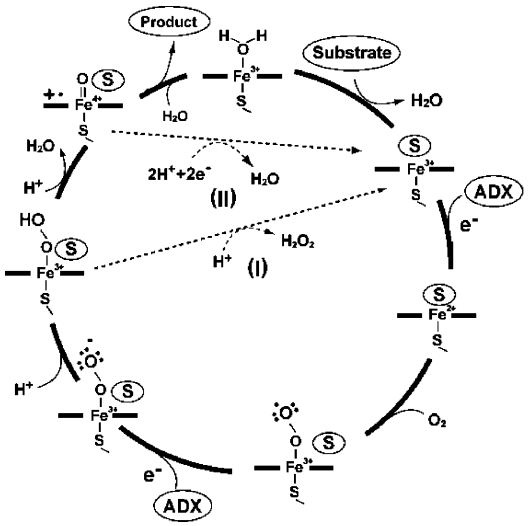

FIGURE 7: Mitochondrial P450 reaction cycle. The uncoupling goes along route I or II, and hydrogen peroxide and/or water are (is) produced instead of the formation of the product.

10-fold higher molar concentration of ADX than ADR showed the highest activity (data not shown), 1α-hydroxylation activity toward 25(OH)D_3 of the wild type and mutants CYP27B1, R458K, and R458Q was measured in the reconstitution system containing various amounts of ADX and ADR at a ratio of 10:1. Figure 6 shows the ADX dependency of catalytic activity of wild type, R458K, and R458Q. Wild type and R458Q showed Michaelis−Menten-type kinetics with the equation $v = V_{max}[ADX]/(K_m + [ADX])$. The kinetic parameters, K_m and k_{cat}, were calculated to be 9.5 μM and 10.4 min^{-1} for the wild type and 347 μM and 0.80 min^{-1} for R458Q, respectively, by the nonlinear regression analysis (Table 3). Thus, both a remarkable increase of K_m and decrease of k_{cat} were observed in R458Q. On the other hand, the kinetic data of R458K were fitted to Hill's equation $v = V_{max}[ADX]^n/(K_m{}^n + [ADX]^n)$, and Hill's constant n was estimated to be 2.0. These results strongly suggest that R458K needs binding of two ADX molecules for 1α-hydroxylation activity.

DISCUSSION

CYP27B1 catalyzes the 1α-hydroxylation of 25(OH)D_3 to produce 1α,25(OH)$_2D_3$. This monooxygenation reaction requires the interaction of the P450 with its proximal electron donor, ADX, which is responsible for the electron transfer from ADR to CYP27B1. In this study, we examined the interaction of CYP27B1 with ADX using site-directed mutagenesis and molecular modeling to identify the amino acid residue of CYP27B1 responsible for interaction with ADX.

The molecular modeling presented in this paper indicates that the four positively charged residues located on the proximal surface of mouse CYP27B1, Lys370 and Lys374 in the K-helix and Arg457 and Arg458 in the L-helix, are involved in electrostatic interaction with the four negatively charged amino acid residues of ADX, Asp72, Glu74, Asp76, and Asp79. Sequence alignments revealed that the four amino acid residues Lys370, Lys374, Arg457, and Arg458 are highly conserved among all mitochondrial P450s, suggesting that these residues play important roles in interaction with ADX. Wada et al. (*16*) showed that Lys377 and Lys381 of CYP11A1 corresponding to Lys370 and Lys374 of mouse CYP27B1 play essential roles in electrostatic interaction with ADX. On the basis of the difference of affinity for ADX between CYP11A1 and CYP27A1, Pikuleva et al. (*15*) revealed the crucial role of Arg418 of CYP27A1 which is only conserved in the CYP27A1 subfamily.

On the other hand, Usanov et al. (*17*) suggested the essential role of Arg426 of CYP11A1 corresponding to Arg458 of mouse CYP27B1 in interaction with ADX. They also showed that Arg425 of CYP11A1 corresponding to Arg457 of mouse CYP27B1 is involved in the folding of CYP11A1. Computer modeling of CYP27B1 suggests that Arg458 is located at the proximal surface and oriented outside the CYP27B1 molecule, whereas the side chain of Arg457 is oriented inside the CYP27B1 molecule. Our experimental data indicate that Arg457 is involved in protein folding, consistent with a three-dimensional model of CYP27B1. Thus, we focused on Arg458 to reveal its role and function in interaction of CYP27B1 with ADX.

Substrate-induced difference spectra and K_m values for substrate 25(OH)D_3 of wild-type CYP27B1 and mutants indicate that the replacement of Arg458 of mouse CYP27B1 toward Lys or Gln dose not affect the binding of substrate 25(OH)D_3. However, these mutants showed a great decrease of k_{cat} values in 1α-hydroxylation activity for 25(OH)D_3 (Table 2). We expected R458Q to show a dramatic decrease in 1α-hydroxylation activity because this mutant corresponds to R426Q of CYP11A1, whose catalytic activity was dramatically reduced as described by Usanov et al. (*17*). A high K_m value of R458Q for ADX and a decrease of the rate constant of the first electron transfer seem reasonable considering that conversion from Arg to noncharged Gln abolishes the salt-bridge formation with the acidic residue of ADX. Thus, it is possible that the remarkable decrease of the coupling efficiency of R458Q is due to decreased electron pressure based on the weak interaction between R458Q and ADX. The NADPH-dependent reduction rate of heme iron and the coupling efficiency of wild type, R458K, and R458Q, shown in Table 3, appear to be consistent with this assumption. However, we cannot explain the higher activity of R458Q than R458K in Tables 2 and 3 only by electron pressure. Thus, we consider the possibility that Arg458 is also involved in an oxygen transfer reaction. As shown in Figure 6, R458K showed atypical kinetics for ADX concentration with Hill's constant of 2.0, suggesting that two ADX molecules are needed for catalytic activity. Judging from the rate constant of the first electron transfer, reduced ADX binds similarly to ferric R458K as to wild type with somewhat lower affinity. The fact that Arg can form a salt bridge with two hydrogen bonds while Lys can form only one hydrogen bond could explain the lower affinity and slow reduction rate of heme iron. Although we have not measured both the second electron transfer and oxygen transfer reaction rates, the extremely low catalytic activity of R458K in the presence of 1 μM ADX appears not due to slow electron transfer but instead to a slow oxygen transfer reaction after the second electron transfer. Thus, the high catalytic activity of R458K at high ADX concentration appears to be due to the remarkable enhancement of the oxygen transfer reaction by binding two ADX molecules. Figure 8 shows a proposed interaction mechanism of R458K with ADX. When one molecule of reduced ADX binds to oxyferric R458K, an

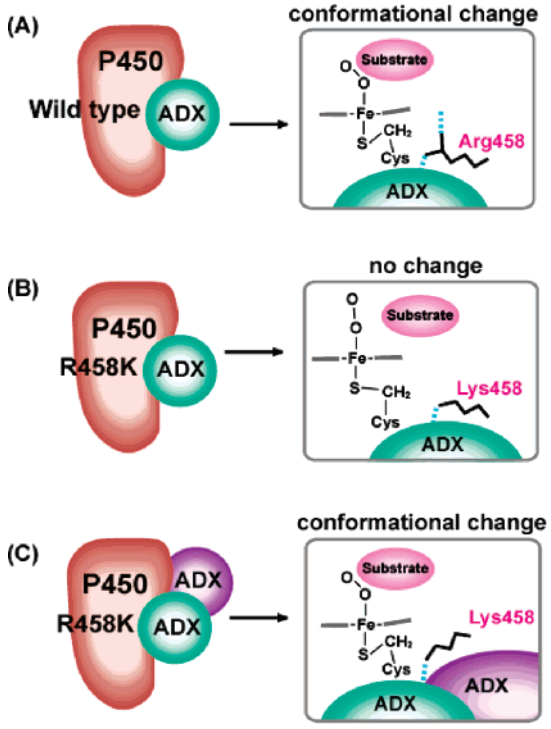

FIGURE 8: Proposed mechanism of interaction between wild-type oxyferric CYP27B1 and reduced ADX (A) and those between oxyferric R458K and one molecule (B) or two molecules (C) of reduced ADX.

oxygen transfer reaction hardly occurs after the second electron transfer. However, if two molecules of reduced ADX bind to oxyferric R458K, an oxygen transfer reaction is promoted, probably by some conformational change of the substrate-binding site of R458K. The coupling efficiency in the presence of 20 μM ADX was estimated to be about 20%, although it is difficult to evaluate coupling efficiency exactly due to the increase of CYP27B1-independent NADPH oxidation. A significant increase of coupling efficiency with increasing ADX concentration strongly suggests a conformational change of the substrate-binding site of R458K. It is unlikely that a dimer of reduced ADX binds to CYP27B1 because reduced ADX prefers monomer formation, whereas oxidized ADX prefers dimer formation (*14*). Recently, Strushkevich et al. (*30*) indicated the presence of another interaction site of CYP11A1 with ADX. Thus, it is possible to assume that R458K has another binding site of reduced ADX to form a 1:2 complex of R458K and ADX. On the other hand, binding one molecule of reduced ADX is sufficient for the conformational change of oxyferric wild-type CYP27B1, judging from its Michaelis−Menten-type kinetics for ADX concentration and high coupling efficiency (Figure 6 and Table 3).

Recent studies on the interaction between P450cam and putidaredoxin revealed that the structure of the substrate-binding site of oxyferric P450cam is changed by the binding of reduced putidaredoxin, and the resultant approach of the substrate *d*-camphor to the heme iron could promote the oxygen transfer reaction (*31*). Thus, putidaredoxin plays an "effector" role in addition to being an electron carrier. Arg112 of P450cam forms a salt bridge with Asp38 of putidaredoxin (*32*), and mutations of Arg112 caused an uncoupling of NADPH oxidation (*33*). Our results in this study strongly suggest that ADX plays an effector role in addition to being an electron carrier like putidaredoxin, and Arg458 of CYP27B1 has a function similar to Arg112 of P450cam. To the best of our knowledge, this is the first report suggesting that ADX functions as an effector upon kinetic studies including measurements of the coupling of NADPH oxidation. As mentioned above, Arg458 of mouse CYP27B1 is conserved in all mitochondrial P450s. Thus, it might be possible to assume that this conserved Arg plays an essential role in the structural change of the substrate-binding site of the oxyferric form of mitochondrial P450 to promote monooxygenation of the substrate.

REFERENCES

1. Boullion, R., Okamura, W. H., and Norman, A. W. (1995) Structure−function relationships in vitamin D endocrine system, *Endocr. Rev. 16*, 200−257.
2. Norman, A. W., Myrtle, J. F., Midgett, R. J., Nowicki, H. G., Williams, V., and Popjak, G. (1971) 1,25-Dihydroxycholestecarciferaol: identification of the proposed active form of vitamin D_3 in the intestine, *Science 173*, 51−54.
3. Lawson, D. E. M., Fraser, D. R. F., Kodicek, E., Morris, H. R., and Williams, D. H. (1971) Identification of 1,25-dihydroxycolestecalciferol, a new kidney hormone controlling calcium metabolism, *Nature 230*, 228−230.
4. Holick, H. L., Schnoes, H. K., and DeLuca, H. F. (1971) 25-Dihydroxycholestecarciferaol, a form of vitamin D_3 metabolically active in the intestines, *Proc. Natl. Acad. Sci. U.S.A. 68*, 803−804.
5. Boyle, I. T., Gray, R. W., and DeLuca, H. F. (1971) 1,25-Dihydroxycolestecalciferol and 21,25-dihydroxycolestecalciferol, *Proc. Natl. Acad. Sci. U.S.A. 68*, 2131−2134.
6. Cali, J. J., and Russell, D. W. (1991) Mutations in the bile acid biosynthetic enzyme sterol 27-hydroxylase underlie cerebrotendinous xanthomatosis, *J. Biol. Chem. 266*, 7774−7778.
7. Cheng, J. B., Motola, D. L., Mangelsdorf, D. J., and Russell, D. W. (2003) De-orphanization of cytochrome P450 2R1: a microsomal vitamin D 25-hydroxylase, *J. Biol. Chem. 278*, 38084−38093.
8. Takeyama, K., Kitanaka, S., Sato, T., Kobori, M., Yanagisawa, J., and Kato, S. (1997) 25-Hydroxyvitamin D_3 1α-hydroxylase and vitamin D synthesis, *Science 277*, 1827−1830.
9. Lambeth, J. D., and Kamin, K. (1979) Ionic effects on adrenal steroidogenic electron transport. The role of adrenodoxin as an electron shuttle, *J. Biol. Chem. 254*, 2766−2774.
10. Lambeth, J. D., Seybert, D. W., Lancaster, J. R., Salerno, J. C., and Kamin, H. (1982) Steroidogenic electron transport in adrenal cortex mitochondria, *Mol. Cell. Biochem. 45*, 13−31.
11. Pikuleva, I., Tesh, K., Waterman, M. R., and Kim, Y. (2000) The tertiary structure of full-length bovine adrenodoxin suggests functional dimmers, *Arch. Biochem. Biophys. 373*, 44−55.
12. Kido, T., and Kimura, T. (1979) The formation of binary and ternary complexes of cytochrome P-450scc with adrenodoxin and adrenodoxin reductase·adrenodoxin complex. The implication in ACTH function, *J. Biol. Chem. 254*, 11806−11815.
13. Hara, T., Koba, C., Takeshima, M., and Sagara, Y. (2000) The formation of binary and ternary complexes of cytochrome P-450scc with adrenodoxin and adrenodoxin reductase.adrenodoxin complex. The implication in ACTH function, *Biochem. Biophys. Res. Commun. 276*, 210−215.
14. Beilke, D., Weiss, R., Lohr, F., Pristovsek, P., Hannemann, F., Bernhardt, R., and Ruterjans, H. (2002) A new electron transport mechanism in mitochondrial steroid hydroxylase systems based on structural changes upon the reduction of adrenodoxin, *Biochemistry 41*, 7969−7978.
15. Pikuleva, I. A., Cao, C., and Waterman, M. R. (1999) An additional electrostatic interaction between adrenodoxin and P450c27 (CYP27A1) results in tighter binding than between adrenodoxin and p450scc (CYP11A1), *J. Biol. Chem. 274*, 2045−2052.
16. Wada, A., and Waterman, M., R. (1992) Identification by site-directed mutagenesis of two lysine residues in cholesterol side chain cleavage cytochrome P450 that are essential for adrenodoxin binding, *J. Biol. Chem. 267*, 22877−22882.
17. Usanov, S. A., Graham, S. E., Lepesheva, G. I., Azeva, T. N., Strushkevich, N. V., Gilep, A. A., Estabrook, R. W., and Peterson, J. A. (2002) Probing the interaction of bovine cytochrome P450scc

(CYP11A1) with adrenodoxin: evaluating site-directed mutations by molecular modeling, *Biochemistry 41*, 8310−8320.
18. Uchida, E., Kagawa, N., Sakaki, T., Urushino, N., Sawada, N., Kamakura, M., Ohta, M., Kato, S., and Inouye, K. (2004) Purification and characterization of mouse CYP27B1 overproduced by an *Escherichia coli* system coexpressing molecular chaperonins GroEL/ES, *Biochem. Biophys. Res. Commun. 323*, 505−511.
19. Yamamoto, K., Uchida, E., Urushino, N., Sakaki, T., Kagawa, N., Sawada, N., Kamakura, M., Kato, S., Inouye, K., and Yamada, S. (2005) Identification of the amino acid residue of CYP27B1 responsible for binding of 25-hydroxyvitamin D_3 whose mutation causes vitamin D-dependent rickets type 1, *J. Biol. Chem. 280*, 30511−30516.
20. Akiyoshi-Shibata, M., Sakaki, T., Ohyama, Y., Noshiro, M., Okuda, K., and Yabusaki, Y. (1994) Further oxidation of hydroxycalcidiol by calcidiol 24-hydroxylase, *Eur. J. Biochem. 224*, 335−343.
21. Yamamoto, K., Masuno, H., Sawada, N., Sakaki, T., Inouye, K., Ishiguro, M., and Yamada, S. (2004) Homology modeling of human 25-hydroxyvitamin D_3 1α-hydroxylase (CYP27B1) based on the crystal structure of rabbit CYP2C5, *J. Steroid Biochem. Mol. Biol. 89*−*90*, 167−171.
22. Sakaki, T., Sawada, N., Takeyama, K., Kato, S., and Inouye, K. (1999) Enzymatic properties of mouse 25-hydroxyvitamin D_3 1α-hydroxylase expressed in *Escherichia coli*, *Eur. J. Biochem. 259*, 731−738.
23. Sawada, N., Sakaki, T., Kitanaka, S., Takeyama, K., Kato, S., and Inouye, K. (1999) Enzymatic properties of human 25-hydroxyvitamin D_3 1α-hydroxylase, coexpression with adrenodoxin and NADPH-adrenodoxin reductase in *Esherichia coli*, *Eur. J. Biochem. 265*, 950−956.
24. Omura, T., and Sato, R. (1964) The carbon monoxide-binding pigment of liver microsomes, *J. Biol. Chem. 239*, 2379−2385.
25. Hiwatashi, A., Nishii, Y., and Ichikawa, Y. (1982) Purification of cytochrome P-450_{D1}α (25-hydroxyvitamin D_3-1α-hydroxylase) of bovine kidney mitochondria, *Biochem. Biophys. Res. Commun. 105*, 320−327.
26. Schiffler, B., Zollner, A., and Bernhardt, R. (2004) Stripping down themitochondrial cholesterol hydroxylase system, a kinetics study, *J. Biol. Chem. 279*, 34269−34276.
27. Tuckey, R. C., McKinley, A. J., and Headlam, M. J. (2001) Placental cytochrome P450scc (CYP11A1): comparison of catalytic properties between conditions of limiting and saturating adrenodoxin reductase, *Eur. J. Biochem. 268*, 2338−2343.
28. Hanukoglu, I., Rapoport, R., Weiner, L., and Sklan, D. (1993) Electron leakage from the mitochondrial NADPH-adrenodoxin reductase-adrenodoxin-P450scc (cholesterol side chain cleavage) system, *Arch. Biochem. Biophys. 305*, 489−498.
29. Rapoport, R., Sklan, D., and Hanukoglu, I. (1995) Electron leakage from the adrenal cortex mitochondrial P450scc and P450c11 systems: NADPH and steroid dependence, *Arch. Biochem. Biophys. 317*, 412−416.
30. Strushkevich, N. V., Azeva, T. N., Lepesheva, G. I., and Usanov, S. A. (2005) Role of positively charged residues Lys267, Lys270, and Arg411 of cytochrome p450scc (CYP11A1) in interaction with adrenodoxin, *Biochemistry (Moscow) 70*, 664−671.
31. Tosha, T., Yoshioka, S., Takahashi, S., Ishimori, K., Shimada, H., and Morishima, I. (2003) NMR study on the structural changes of cytochrome P450cam upon the complex formation with putidaredoxin. Functional significance of the putidaredoxin-induced structural changes, *J. Biol. Chem. 278*, 39809−39821.
32. Shimada, H., Nagano, S., Hori, H., and Ishimura, Y. (2001) Putidaredoxin-cytochrome P450cam interaction, *J. Inorg. Biochem. 83*, 255−260.
33. Unno, M., Shimada, H., Toba, Y., Makino, R., and Ishimura, Y. (1996) Role of Arg112 of cytochrome p450cam in the electron transfer from reduced putidaredoxin. Analyses with site-directed mutants, *J. Biol. Chem. 271*, 17869−17874.

BI060072O